Photoionization efficiency spectroscopy and density functional theory investigations of $RhHo_2O_n$ (n=0–2) clusters

Alexander S. Gentleman, Matthew A. Addicoat,[a] Viktoras Dryza,[b] Jason R. Gascooke,[c] Mark A. Buntine,[d] and Gregory F. Metha[e]
Department of Chemistry, The University of Adelaide, South Australia 5005, Australia

(Received 28 November 2008; accepted 27 March 2009; published online 28 April 2009)

The experimental and theoretical adiabatic ionization energies (IEs) of the rhodium-holmium bimetallic clusters $RhHo_2O_n$ (n=0–2) have been determined using photoionization efficiency spectroscopy and density functional theory (DFT) calculations. Both sets of data show the IE of $RhHo_2O$ to be significantly lower than the values for $RhHo_2$ and $RhHo_2O_2$, which are found to be similar. This indicates that there are significant changes in electronic properties upon sequential addition of oxygen atoms to $RhHo_2$. The DFT investigations show that the lowest energy neutral structures are a C_{2v} triangle for $RhHo_2$, a C_{2v} planar structure for $RhHo_2O$ where the O atom is doubly bridged to the Ho–Ho bond, and a C_{2v} nonplanar structure for $RhHo_2O_2$, where the O_2 is dissociative and each O atom is doubly bridged to the Ho–Ho bond in the cluster above and below the $RhHo_2$ trimer plane. Good correlation between the experimental and computational IE data imply that the lowest energy neutral structures calculated are the most likely isomers ionized in the molecular beam. In particular, the theoretical adiabatic IE for the dissociative $RhHo_2O_2$ structure is found to compare better with the experimentally determined value than the corresponding lowest energy O_2 associative structure. © *2009 American Institute of Physics*. [DOI: 10.1063/1.3120442]

I. INTRODUCTION

Transition metal oxides have been the topic of intense research over the last few decades due to their widespread use in the area of heterogeneous catalysis. Industrially significant reactions such as the partial oxidation of methane gas (POX) and various others can be catalyzed using transition metal oxides.[1–4] In an attempt to understand the mechanistic workings behind these catalysts, transition metal oxide clusters have been used as models for solid-state oxide surfaces. Reactant molecules (e.g., methane in the POX process) can be made to interact with various metal oxide clusters and an overall understanding of how the molecules are activated in the catalytic process can be achieved. For example, Fu *et al.*[5–7] performed density functional theory (DFT) studies using the Mo_3O_9 and Cr_3O_9 clusters as catalytic models to understand the mechanistics of C–H bond activation of methane and propane in various processes, including the POX process.

Furthermore, it has been shown that transition metal oxide clusters can also act as catalysts in the gas phase. In a recent review,[8] it has been reported that anionic Au-oxide and Pt-oxide clusters serve as good catalysts for the oxidation of CO to CO_2.[9–11] Other processes, such as the conversion of primary and secondary alcohols to aldehydes and ketones, were also found to be catalyzed by the protonated dimolybdate anion cluster, $[Mo_2O_6(OH)]^-$.[12] Thus, transition metal oxide clusters clearly provide an exciting field of study with respect to catalysis.

However, most catalytic investigations involving transition metal oxide clusters have been limited to homonuclear metal oxide clusters. It is well known that adding differing types of metals to catalytic metal surfaces can enhance certain industrial processes such as CO oxidation and alkane hydrolysis.[13] Therefore, adding metal heteroatoms to transition metal oxide clusters allows the possibility of tailoring the composition of the cluster to provide optimal catalytic activity. Despite this, very little is known about the structures of bimetallic cluster oxides. Of the few studies, Janssens *et al.* performed infrared multiple photon dissociation spectroscopy in combination with DFT on various titanium-vanadium oxide cluster anions to investigate how the electronic and geometric structures change by exchanging V atoms with Ti atoms.[14]

Another variety of bimetallic oxide clusters that remains to be investigated are those composed of transition and lanthanide metal atoms. It has been found that doping transition metal oxide catalysts with lanthanide metal atoms can promote catalytic activity in industrial processes (again, with the POX process) with greater conversion and selectivity.[4,15] Therefore, transition-lanthanide bimetallic oxide clusters have the potential to be very efficient and selective catalysts in various industrial processes.

Despite a great deal of previous experimental and com-

[a]Present address: Research School of Chemistry, Australian National University, Canberra, ACT, 0200.
[b]Present address: School of Chemistry, University of Melbourne, Melbourne, Victoria, 3010.
[c]Present address: School of Chemistry, Physics and Earth Sciences, Flinders University, South Australia 5042, Australia.
[d]Present address: Department of Applied Chemistry, Curtin University of Technology, Perth, Western Australia 6845, Australia.
[e]Author to whom correspondence should be addressed. Present address: Department of Chemistry, The University of Adelaide, South Australia 5005, Australia. Tel.: +61 8 8303 5943. FAX: +61 8 8303 4358. Electronic mail: greg.metha@adelaide.edu.au.

putational studies on gas-phase lanthanide and lanthanide oxide clusters,[16–26] very little work has been done on transition-lanthanide bimetallic clusters and their oxides. Zhang *et al.*[27] performed DFT investigations on Ni- and Ti-doped La_{13} clusters where they found that substituting a La atom with a Ni or Ti atom lowered the binding energy of the cluster as a whole (relative to La_{13}), where Ni preferred to occupy a surface site and Ti preferred to occupy a central site. In addition to this, Liu *et al.*[28] performed DFT calculations on La_mNi_n $(m+n \leq 7)$ bimetallic clusters, reporting the lowest energetic isomers for each respective cluster. In the 1970s, Cocke and Gingerich[29,30] produced the dimers AgHo, AuHo, and CePd in the gas phase and determined their dissociation energies, standard heats of formation, and appearance potentials. More recently, Lievens and co-workers generated gas-phase Au_nEr^+ $(3 \leq n \leq 20)$ clusters and performed stability and dissociation pathway analyses on them.[31] They found that Au_6Er^+ and $Au_{16}Er^+$ were exceptionally stable due to them both containing 8 and 18 itinerant valence electrons, respectively, which afford closed electronic shell structures for each of these species.[31] However, no specific inferences were made about whether there are geometric changes induced by Er-doping of the Au clusters. With respect to reactivity, Huang and Freiser[32] investigated the reactivity of the $LaFe^+$ dimer toward alkanes. It was observed that this dimer can dehydrogenate two ethane molecules sequentially, whereas the separate cationic atoms are either nonreactive toward ethane (Fe^+) or can only dehydrogenate one ethane molecule (La^+). With respect to work performed on the oxides of transition-lanthanide bimetallic clusters, Gibson[33] produced these types of clusters in the gas phase via the laser ablation of oxalates into vacuum. It was proposed that ZrO_2 and HfO_2 act as coordinating ligands to the basic cluster structure of various lanthanum oxide clusters. These transition-lanthanide oxide clusters were proposed to form cubic structures based on the crystal structures of lanthanide monoxides. However, no computational work was performed to verify the proposed structure for each cluster.

Clearly, there is still much to be learned about the structure and reactivity of transition-lanthanide bimetallic clusters and their oxide counterparts. In particular, it would be of significant interest to understand the oxide chemistry of these types of clusters by investigating where the oxygen atoms prefer to bind and how this affects the electronic properties. In an attempt to do this, we used photoionization efficiency (PIE) spectroscopy to determine the adiabatic ionization energies (IEs) of the $RhHo_2O_n$ $(n=0-2)$ bimetallic oxide cluster series. Rhodium was chosen as the transition metal as it is catalytically relevant in the cluster regime.[34–39] Due to the fact that the chemical properties across the lanthanide series are generally thought to be similar,[40] pragmatic reasons were used to select the lanthanide metal. Therefore, holmium was chosen as the lanthanide metal due to it being monoisotopic, thus minimizing complications in the mass spectra. The experimental IEs show how the sequential addition of oxygen atoms affects the electronic properties of the $RhHo_2$ cluster and comparison with values predicted by DFT allows geometric information to be inferred. From this, we have also been able to show that the lowest energy structure of $RhHo_2O_2$ has the O_2 bound dissociatively, not associatively, to the $RhHo_2$ cluster.

II. EXPERIMENTAL AND COMPUTATIONAL METHODS

A. Experimental method

The holmium-rhodium and oxide clusters are produced in the gas phase using a dual laser ablation source coupled to a Wiley–McLaren time-of-flight mass spectrometer (TOF-MS). The ablation source used is similar in design to that used by Kaya and co-workers[41] to generate various types of bimetallic clusters in the gas phase and investigate their reactivity with small molecules. As the experimental details of the dual ablation source have not been described previously, a general description is given below.

Pure helium carrier gas (CIG gases 99.98%) with a backing pressure of 60 psi is delivered into a 3 mm ablation channel via a pulsed nozzle (General Valve, Series 9, 20 μm) driven by a home-made nozzle driver. The metal rods readily oxidize and have sufficient amounts of metal oxides inherently present to lead to the formation of oxide clusters. Holmium and rhodium metal rods (DXL, 99.9%) are ablated independently with two separate neodymium-doped yttrium aluminum garnet (Nd:YAG) lasers (Big Sky Laser, ULTRA-CFR, 10 Hz, 532 nm) focused onto the rods with 250 mm focal length lenses. Typical ablation powers used are 12 mJ for the holmium rod and 2 mJ for the rhodium rod. Optimal signal of the bimetallic clusters was achieved when the rhodium rod was ablated 4 μs after the holmium rod. A screw mechanism (Oriel, motor-mike 18014) constantly rotates and translates both metal rods to ensure that a fresh surface is ablated. The ablated products entrained in the helium carrier gas are then passed into a fast-flow reactor channel, which has a length of 60 mm and an internal diameter tapering outwards from 2 to 5 mm at the start of the channel. The clusters then pass through a 30 mm long "condensation tube" with an internal diameter of 2 mm to facilitate further clustering. Upon reaching the end of the condensation tube, the clusters supersonically expand into a second chamber that contains a Wiley-McLaren TOF-MS, which is arranged perpendicularly to the molecular beam. Upon supersonic expansion, the internal vibronic temperature of all clusters formed in the ablation process is ~300 K, as reported in our previous papers.[42,43] The neutral clusters formed in the laser ablation process are ionized with the frequency doubled output of a Nd:YAG pumped dye laser (220–280 nm) and extracted perpendicularly using deflection plates and an Einzel lens into the TOF-MS flight region and onto a double microchannel plate detector. The resulting cluster signal is then amplified ×25 with a commercial preamplifier (Stanford SR445) and delivered to a digital oscilloscope (LeCroy 9350 a.m., 500 MHz) for averaging (1000 laser shots) before being sent to a PC for analysis.

The specific details of the PIE experiments are similar to those that have been reported previously.[44] Briefly, all data points in the PIE experiments are collected at 0.25 nm intervals. Typical laser powers used are around 80 μJ/pulse, collimated to a 5 mm-diameter beam, as measured using a py-

roelectric powermeter (Ophir Nova II). Under these conditions, all ion signals are found to be linearly dependent with laser fluence. During each wavelength, the laser power is kept constant. To check that long-term intensity fluctuation had not occurred, the laser is returned to the starting wavelength immediately after each scan to ensure that the cluster signal intensity remained constant.

III. COMPUTATIONAL PROCEDURE AND DETAILS

Geometry optimization and harmonic vibrational frequency calculations were performed using DFT in the GAUSSIAN 03 suite of programs.[45] The B3P86 density functional method was used with the SDD basis set to locate as many geometric isomers as possible for the $RhHo_2O_n$ (n=0–2) clusters. The holmium atoms in the clusters were treated with an extended Stuttgart–Dresden effective core potential (ECP) developed by Dolg *et al.*,[46–49] which treated the 4*f* electrons as part of the ECP (denoted SDD^{+}). The conventional SDD basis set was used on the rhodium and oxygen atoms. Starting geometries for $RhHo_2$ consisted of differing types of linear and triangular configurations. Starting geometries for $RhHo_2O$ consisted of the oxygen atom interacting with a holmium or rhodium atom, a Ho–Rh or Ho–Ho edge, or all three atoms in the optimized structure of the $RhHo_2$ trimer base. Starting geometries for $RhHo_2O_2$ consisted of the O_2 molecule interacting associatively (O_2 molecule intact) or dissociatively (two separate O atoms) with the optimized structure of the $RhHo_2$ trimer base. Among the associatively bound starting geometries, the O_2 molecule was made to interact with the $RhHo_2$ cluster singly bound to either a holmium or rhodium atom, doubly bound to either a Ho–Rh or Ho–Ho edge, or triply bound to all three atoms. The dissociatively bound starting geometries contained various combinations of the two separate oxygen atoms being singly bound to either a holmium or rhodium atom, doubly bound to either the Ho–Rh or Ho–Ho edge, or triply bound to all three atoms in the $RhHo_2$ cluster. Doublet, quartet, sextet, and octet multiplicities were considered for the neutral species and singlet, triplet, quintet, and septet multiplicities were considered for the cationic species. We are confident that a thorough investigation of the potential energy surface of each cluster was performed and that the lowest energy neutral and cationic structures reported are indeed the global minima for each cluster. All initial optimizations were performed with no constraints on symmetry. Harmonic vibrational frequency calculations were then performed on all unique structures to determine if they were true minima (no imaginary frequencies). If the global minima possessed higher symmetry, reoptimization within symmetric constraints is performed and the energetics are compared with the initial structures to ensure that there was no significant deviation. This was done in order to properly analyze and assign the vibrational modes and the ground states of each cluster. Stability tests were also performed on the corresponding wave functions of all the global minima. Structural information for each respective cluster is located in the supplementary material.[50]

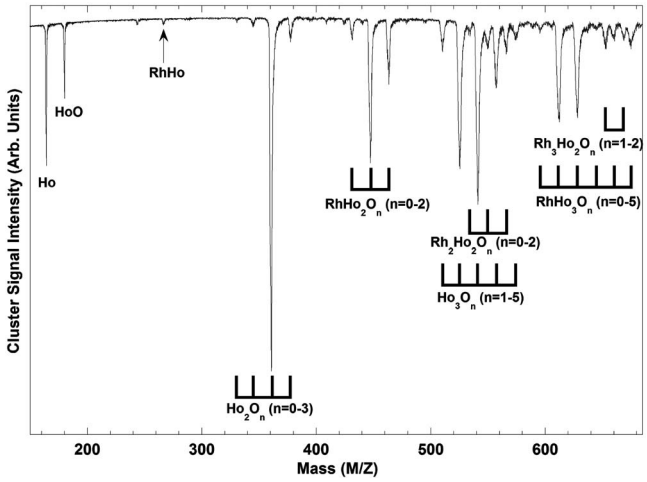

FIG. 1. Mass spectrum of various holmium and rhodium-holmium bimetallic clusters and their oxides recorded at 222 nm under single photon ionization conditions.

IV. RESULTS AND DISCUSSION

A. Mass spectra and photoionization measurements

Figure 1 shows a time-of-flight mass spectrum of holmium oxide and holmium-rhodium bare and oxide clusters recorded at 222 nm under single-photon ionization conditions. As seen in the spectrum, holmium oxide clusters of the form Ho_2O_n (n=0–3) and Ho_3O_n (n=1–5) were generated in abundance. The Ho_2 dimer was found to form with very little intensity. The Ho_3 trimer did not appear in the mass spectrum. The lack of aggregation of holmium clusters has been observed previously by Nagao *et al.*[20,21] and was attributed to the Coulombic repulsion that arises from their ability to act as three-electron donors. Also observed in Fig. 1 are the holmium-rhodium clusters $RhHo_2O_n$ (n=0–2), $Rh_2Ho_2O_n$ (n=0–2), and $RhHo_3O_n$ (n=0–5). Rhodium dominated species, such as Rh_2HoO_n and Rh_3HoO_n, were not present in the mass spectrum. This is due either to them not being present in the molecular beam or that the ionization wavelength is below the IE of the clusters. Due to the fact that $Rh_3Ho_2O_n$ (n=1–2) clusters appeared in the mass spectrum at 222 nm, we contend that the latter reason accounts for their nonappearance. In this paper, only the PIE data for $RhHo_2O_n$ (n=0–2) clusters will be discussed together with detailed computational work. An analysis of the $Rh_2Ho_2O_n$ (n=0–2) and $RhHo_3O_n$ (n=0–5) clusters awaits the completion of computational work and will be published elsewhere.

Figures 2(a)–2(c) show the portion of the mass spectrum containing the $RhHo_2O_n$ (n=0–2) clusters, which were recorded with three different ionizing wavelengths: 262, 242, and 222 nm. Each of these mass spectra was recorded under identical and single-photon ionization conditions. In the spectrum at 222 nm [Fig. 2(c)], it is clearly seen that all three clusters appear with moderate to high intensities. The cluster $RhHo_2O$ has the most intense peak, followed by $RhHo_2O_2$ then $RhHo_2$. Ionization at 242 nm [Fig. 2(b)] yields only $RhHo_2O$, with a slight decrease in intensity. At 262 nm [Fig. 2(a)], it is seen that all signals decreased to baseline, implying that none of the species are ionized at this wavelength.

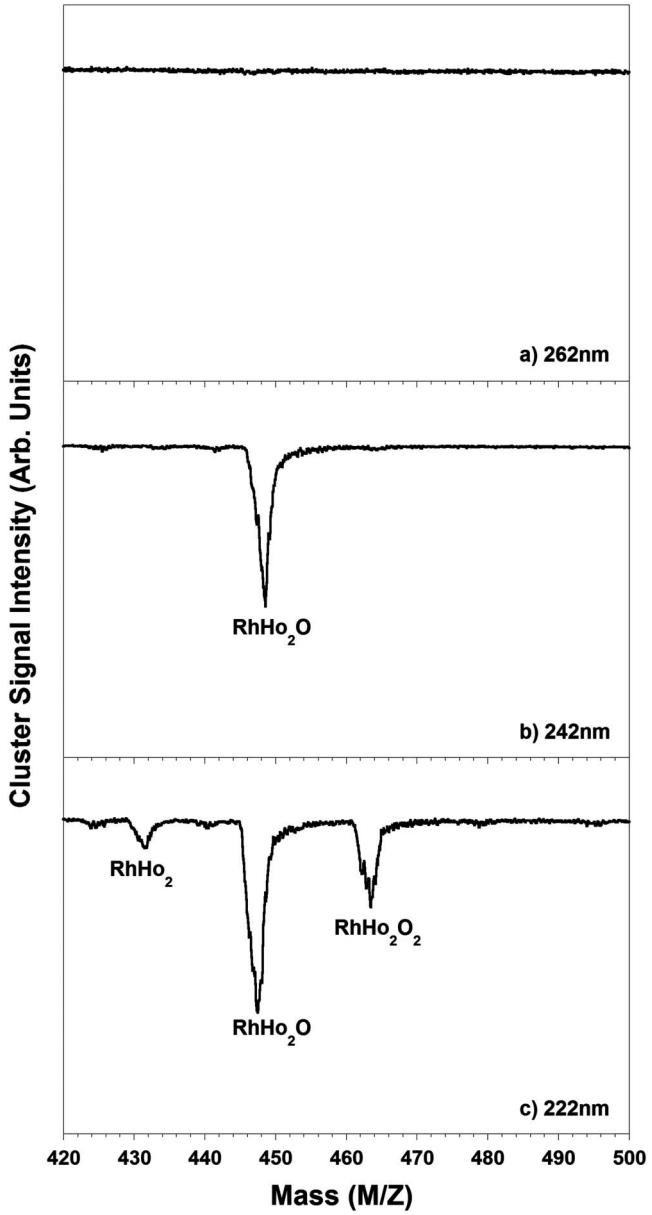

FIG. 2. Mass spectra of the $RhHo_2O_n$ (n=0–2) clusters recorded at three different ionization wavelengths: (a) 262, (b) 242, and (c) 222 nm.

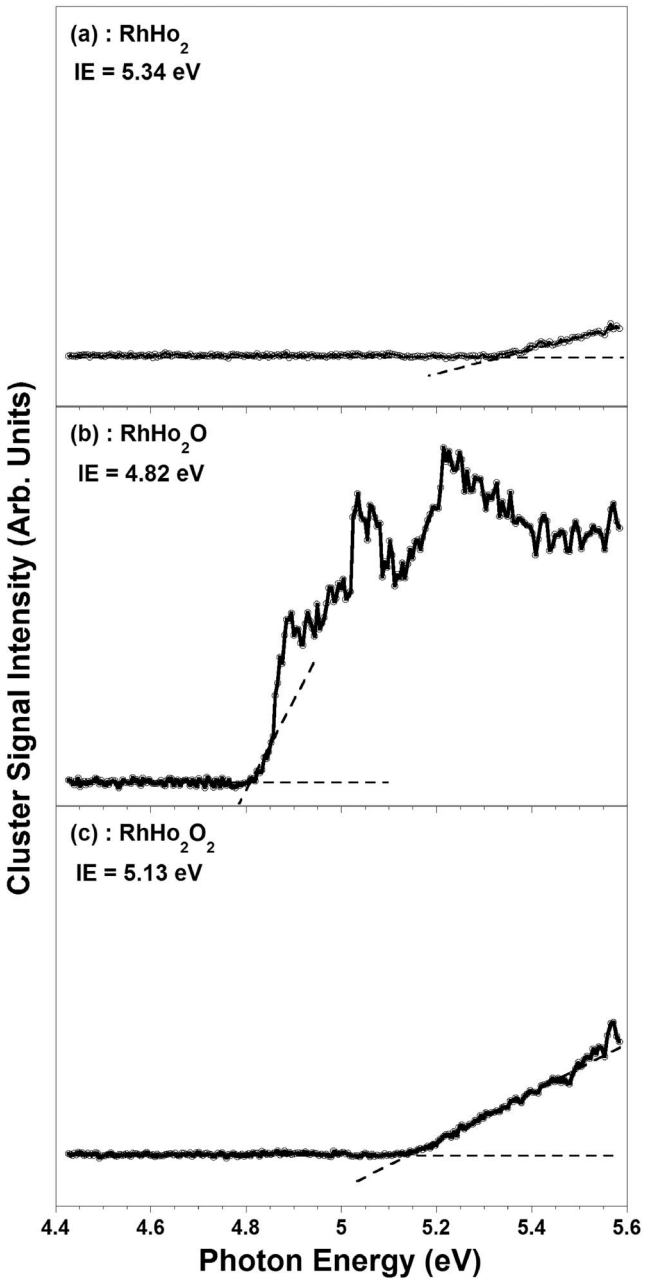

FIG. 3. PIE spectra of the $RhHo_2O_n$ (n=0–2) clusters. The determined IEs are also displayed (uncertainty in IEs= ±0.05 eV).

The PIE spectra were recorded by monitoring the cluster signal as a function of wavelength. The PIE spectra for the $RhHo_2O_n$ (n=0–2) species are shown in Figs. 3(a)–3(c), respectively. $RhHo_2O$ shows a dramatic increase in intensity from baseline, signifying good Franck–Condon (FC) overlap between the electronic states of the neutral and the cation and is indicative of little or no geometric change. The PIE spectrum for this species levels off after 5.4 eV, satisfying that the highest energy FC-allowed transition was attained. Interestingly, the PIE spectrum for this species displays structure before leveling off, which is not usually observed for molecules this large. We confirmed that this is not due to a change in cluster abundance as PIE curves of other, simultaneously recorded species with low IEs (i.e., $RhHo_3O_2$) did not show this behavior. Contrary to $RhHo_2O$, the PIE spectra for $RhHo_2$ and $RhHo_2O_2$ show very gradual onsets of ionization from baseline, signifying poor FC overlap between the neutral and the cation for these two species. The PIE curves for these two species also show no leveling off after 5.6 eV (222 nm) toward the higher energy parts, indicating that the highest FC-allowed transition has not yet been attained.

The method we use to determine the IEs has been described previously.[44] Briefly, two lines are fitted to the baseline and the linear rise of the signal. The intersection of these two lines is denoted as the appearance potential of the cluster and from this, the adiabatic IEs of the $RhHo_2O_n$ (n=0–2) clusters are determined. This procedure of IE determination has an estimated error of ±0.05 eV associated with it. Figures 3(a)–3(c) also show the experimentally determined adiabatic IEs for the $RhHo_2O_n$ (n=0–2) clusters. The IE for $RhHo_2$ was determined to be 5.34 eV, which is low for a Rh

TABLE I. List of the various parameters of Ho_2, HoO, RhO, and HoRh calculated using the B3P86 density functional and the SDD and SDD† basis sets (see text for details). Also listed are the experimentally and theoretically known parameters for the pertinent dimers.

Dimer	Calc. ω_e (cm^{-1})	Known ω_e (cm^{-1})	Calc. r (Å)	Previously calc. r (Å)	Calc. bond strength (eV)	Known bond strength (eV)	Calc. IE (eV)	Known IE (eV)
Ho_2	118.1	112.0[a] 135.2[b]	3.176	3.317[a]	1.24	0.87 ± 0.18[b]	5.76	6.0 ± 1.0[b]
HoO	855.4	839[c] 828.1[d] 834[g]	1.788	1.792[c]	7.33	5.12[c] 6.33 ± 0.18[e]	6.84	7.372[c] 6.1 ± 0.5[f] 6.2 ± 0.1[h]
RhO	827.1	838.3[i] 799.0[i]	1.745	1.739[i] 1.887[l]	3.84	4.15 ± 0.43[j]	9.71	8.63 ± 0.43[k]
HoRh	322.6	⋯	2.711	⋯	4.81	⋯	7.07	⋯

[a]Reference 52.
[b]Reference 29.
[c]Reference 24.
[d]Reference 53.
[e]Reference 55.
[f]Reference 56.
[g]Reference 54.
[h]Reference 57.
[i]Reference 58.
[j]Reference 59.
[k]Reference 60.
[l]Reference 61.

containing cluster considering that pure Rh clusters are known to have very high IEs (Rh_{1-4}, IE =6.42–7.87 eV, Rh_{5-18}, IE<6.42 eV).[51] The addition of an oxygen atom to the $RhHo_2$ bare metal cluster to yield $RhHo_2O$ results in the IE changing by −0.52 eV. The addition of a second oxygen atom then results in an IE change of +0.31 eV. In comparing the IEs of $RhHo_2$ and $RhHo_2O_2$, it is observed that the addition of two oxygen atoms changes the IE by only −0.19 eV.

B. DFT calculations

1. Justification of basis set

In order to explain the observed trend in experimental IEs, DFT calculations were performed on the neutral and cationic $RhHo_2O_n$ (n=0–2) clusters. Since f-electrons of lanthanide atoms are known to take little to no part in chemical interaction and can make calculations very complicated and time consuming, a $4f^n/Q$=11 quasirelativistic pseudopotential version of the Stuttgart–Dresden (denoted SDD†) basis set developed by Dolg *et al.*[46–49] was used for the lanthanide atoms. For Ho, in the $[Xe]4f^{10}6s^25d^1$ electron configuration, all electrons apart from the 5s, 5p, 6s, and 5d are taken into the pseudopotential. The $4f^n/Q$=11 notation denotes the number of f-electrons (n) and the number of valence electrons (11) considered for the calculations involving the Ho atom. Thus, the SDD† basis set on holmium affords a valence electron configuration of $5s^25p^66s^25d^1$. This basis set has been used by Nemukhin *et al.*[52] for the Ho_2 cluster, where various *ab initio* methods were used (with the $4f^n/Q$=11 pseudopotential) to predict and assign the optical UV-visible (UV-vis) spectral transitions observed for Ho_2 suspended in an argon matrix. They found that the predicted UV-vis transitions correlated extremely well with the experimentally observed transitions, thus confirming the assumption that f-electrons play no significant part in chemical interaction and that the SDD† basis set is suitable to predict and verify experimental data.

The SDD† basis set was used only for the holmium atoms in this paper and the standard SDD basis set was used on rhodium and oxygen atoms. Therefore, it was necessary to benchmark the use of the SDD†/SDD basis set (in combination with the B3P86 density functional) against known parameters for pertinent diatomic molecules containing all three atoms.

To test this, three diatomic molecules were chosen to benchmark against HoO, Ho_2, and RhO. These were chosen as they have known parameters and chemical bonds relevant to the $RhHo_2O_n$ (n=0–2) clusters. Table I shows various experimental[29,53–60] and previously calculated[24,52,58,61] parameters of Ho_2, HoO, and RhO, in addition to our calculated parameters. Even though there are no known experimental parameters for HoRh, the geometry of this dimer was also calculated so that relative bond strengths could be compared to the other three diatomics. All the calculated parameters were found to compare extremely well with experimental values. Notably good agreement between experiment and theory are obtained for the ω_e and r values, which deviate by no more than ~30 cm^{-1} and 0.150 Å, respectively. Of the other parameters, the calculated D_o and IE values are also in reasonable agreement with the known parameters. In the case of HoO, the IE calculated using the SDD†/SDD basis set compares better with experimental values than that calculated by Wu *et al.*[24] Thus, the SDD†/SDD basis set is justified for use with $RhHo_2O_n$ (n=0–2) clusters.

2. Neutral and Cationic Geometries of $RhHo_2O_n$ (n=0–2)

The lowest energy structures and Mulliken charges of all atoms for the neutral and cationic isomers of $RhHo_2O_n$ (n=0–2) are shown in Fig. 4.

a. $RhHo_2$ For the neutral and cationic $RhHo_2$ species, the lowest energy neutral structure was determined to be a doublet C_{2v} isosceles triangle in the $^2A_1$ state (structure **IA**) with Ho–Ho and Ho–Rh bond lengths of 3.498 and 2.386 Å, respectively. The lowest energy cationic structure was determined to be a singlet C_{2v} isosceles triangle in the $^1A_1$ state (Structure $\mathbf{IA}^+$) with Ho–Ho and Ho–Rh bond lengths of 3.923 and 2.380 Å, respectively. Other neutral and cationic minima were also calculated, but were found to be much

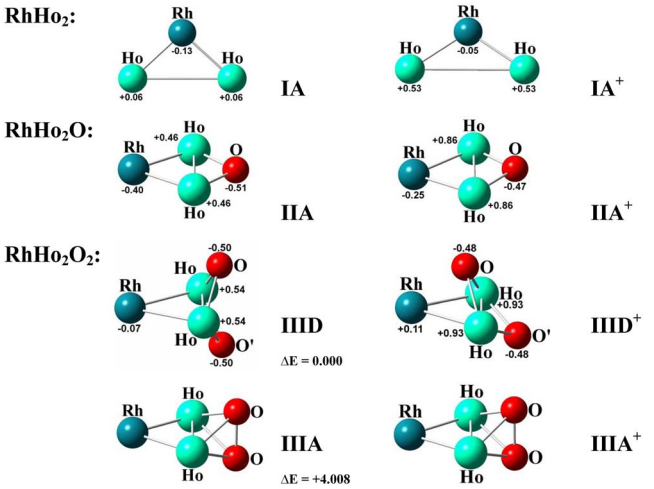

FIG. 4. (Color online) Structures of the calculated isomers of neutral and cationic $RhHo_2O_n$ (n=0–2) clusters. For $RhHo_2O_2$, the lowest energy associative and dissociative structures and their energies relative to each other (ΔE in eV) are shown. The Mulliken charges of each atom in the clusters are also displayed.

higher in energy. Upon ionization, the rhodium and holmium atoms gain a net charge of +0.08 and +0.47, respectively (refer to Mulliken charges in Fig. 4). The increased electrostatic repulsion experienced between the two Ho atoms causes the Ho–Ho bond length to increase by 0.425 Å in the cationic structure. This bond length change is significant and indicates that there is significant motion along one of the FC coordinates. This is consistent with the PIE curve of $RhHo_2$ [Fig. 3(a)], which exhibits a slow onset of ionization.

Due to the scarcity of computational work on bare transition-lanthanide metal trimers, the only comparison that can be made is with the DFT structures of bare lanthanum-nickel bimetallic clusters determined by Liu *et al.*[28] In their work, the neutral $NiLa_2$ trimer was found to be a singlet C_{2v} isosceles triangle with bond lengths of La–Ni and La–La being 2.555 and 3.050 Å, respectively. In comparison to the neutral structure of $RhHo_2$, both clusters were determined to have C_{2v} symmetry with the lanthanide dimer bond lengths being longer than the transition-lanthanide metal bond lengths. To the best of our knowledge, no published work exists on cationic transition-lanthanide bimetallic clusters.

b. $RhHo_2O$ For the neutral $RhHo_2O$ species, the lowest energy structure is a planar doublet C_{2v} structure in the $^2B_2$ state with the O atom bound across the Ho–Ho bond (structure **IIA**). The lowest energy cationic structure was found to be a singlet C_{2v} structure in the $^1A_1$ state with the O atom bound in the same manner (structure **IIA**$^+$). Both structures are consistent with increased stability of the Ho–O bond relative to the Rh–O bond (refer to bond strengths in Table I), which results in the oxygen atom binding to the Ho–Ho edge rather than the Ho–Rh edge. Higher multiplicities of the neutral and cationic $RhHo_2O$ minima were found to be much higher in energy. Upon ionization from structure **IIA** to **IIA**$^+$ ($^1A_1 \leftarrow {}^2B_2$), the holmium, rhodium, and oxygen atoms all gain a net charge of +0.40, +0.15, and +0.04, respectively. Despite the significant gain in positive charge by the holmium atoms, the Ho–Ho bond length decreases by 0.04 Å. The Ho–O and Ho–Rh bond lengths also decreased by 0.02 and 0.01 Å, respectively. The slight shortening of the latter two bonds, attributed to increased electrostatic interaction, keeps the cationic structure rigid and inhibits the lengthening of the Ho–Ho bond upon ionization. All these structural changes are relatively small and indicate strong FC overlap between the neutral and cationic structures. This is entirely consistent with the PIE curve for $RhHo_2O$ [Fig. 3(b)], which exhibits sharp onset following ionization. Due to the lack of work that currently exists on transition-lanthanide bimetallic monoxides, no direct comparison with these types of mixed metal oxide systems is possible.

c. $RhHo_2O_2$ For the neutral $RhHo_2O_2$ species, the lowest energy structure is a doublet nonplanar C_{2v} structure in the $^2A_1$ state with each individual oxygen atom doubly bridged to a Ho–Ho bond (structure **IIID**). The lowest energy neutral structure with associatively bound O_2 was found to be a doublet C_{2v} structure in the $^2B_1$ state with O_2 bound perpendicular to the $RhHo_2$ trimer base across the Ho–Ho bond (structure **IIIA**). This structure is +4.01 eV higher in energy than the dissociative structure. The lowest energy cationic structure was found to be a singlet nonplanar C_s dissociative structure in the $^1A'$ state with each individual oxygen atom doubly bound to the Ho–Ho bond (structure **IIID**$^+$). One of the oxygen atoms migrated toward the rhodium atom, thus differentiating it from **IIID**. The lowest energy cationic structure with associatively bound O_2 was found to be a singlet C_{2v} structure in the $^1A_1$ state with a structural motif very similar to that of **IIIA** (structure **IIIA**$^+$). As with $RhHo_2O$, the increased stability of the Ho–O bond compared to the Rh–O bond results in the oxygen atoms binding to the Ho–Ho edge rather than the Ho–Rh edge in both the neutral and cationic structures. Other neutral and cationic minima at higher multiplicities were calculated but were found to lie much higher in energy than those presented here. Due to the fact that structure **IIID** is significantly lower in energy than structure **IIIA**, we contend that only structure **IIID** is present in our experiment. Upon ionization from structure **IIID** to structure **IIID**$^+$ ($^1A' \leftarrow {}^2A_1$), the holmium, rhodium, and oxygen atoms gain a net charge of +0.39, +0.18, and +0.02, respectively. It is worth noting that the gain in net charge by the rhodium atom causes it to become positively charged ($-0.07 \rightarrow +0.11$). Since both oxygen atoms are negatively charged, the acquisition of this positive charge causes a 44.6° dihedral angle shift of one of the oxygen atoms (labeled O in Fig. 4) toward the rhodium atom via electrostatic attraction. Despite being negatively charged, the other oxygen atom (labeled O′ in Fig. 4) shifts away from the rhodium atom by a dihedral angle change of 34.1°. Another minimum in which both oxygen atoms shift toward the rhodium atom was located but was 2.75 eV higher in energy than structure **IIID**$^+$ (structure **IIID2**$^+$ in the supplementary material). These are significant structural changes and suggest poor FC overlap between the lowest energy neutral and cationic structures. This is consistent with the PIE curve of $RhHo_2O_2$ [Fig. 3(c)], which exhibits a slow onset of signal following ionization. As with $RhHo_2O$, there is no previous work on the oxides of transition-lanthanide bimetallic clusters and so no direct comparison is possible.

TABLE II. List of the experimental IEs determined for the $RhHo_2O_n$ (n=0–2) clusters. Also shown are the transitions and IEs (offset and excluding ZPE) calculated using the B3P86 density functional and the SDD/SDD† basis set (uncertainty in IEs= ±0.05 eV).

Cluster	Expt. IE	Structure	Calc. transition	Calc. IE (excluding ZPE)	Offset IE
$RhHo_2$	5.34	IA	$^1A_1 \leftarrow {}^2A_1$	5.80	5.34
$RhHo_2O$	4.82	IIA	$^1A_1 \leftarrow {}^2B_2$	5.37	4.91
$RhHo_2O_2$	5.13	IIID	$^1A' \leftarrow {}^2A_1$	5.66	5.20
		IIIA	$^1A_1 \leftarrow {}^2B_1$	5.40	4.94

C. Theoretical adiabatic IEs of $RhHo_2O_n$ (n=0–2)

The ionization transition between the neutral and cationic structures of the $RhHo_2O_n$ (n=0–2) clusters obeying the $\Delta S = \pm(1/2)$ selection rule is considered. The energy difference (in eV) between the lowest energy neutral and cationic isomers is calculated to be the adiabatic IE of each cluster. These values for the $RhHo_2O_n$ (n=0–2) clusters (including the associative and dissociative structures of $RhHo_2O_2$) are listed in Table II.

Upon the $^1A_1 \leftarrow {}^2A_1$ transition for $RhHo_2$, the theoretical adiabatic IE for $RhHo_2$ was determined to be 5.80 eV. The addition of an oxygen atom to the bare metal cluster decreases the IE by 0.43 eV, yielding an adiabiatic IE of 5.37 eV upon the $^1A_1 \leftarrow {}^2B_2$ transition for $RhHo_2O$. The addition of another oxygen atom increases the IE by 0.29 eV, yielding an IE of 5.66 eV for the $^1A' \leftarrow {}^2A_1$ transition of the dissociative $RhHo_2O_2$ structure. The adiabatic IE for the corresponding lowest energy associative structure is 5.40 eV for the $^1A_1 \leftarrow {}^2B_1$ transition.

These results show that an IE change is predicted following the addition of one oxygen atom to $RhHo_2$. This is indicative of some change in the electronic structure of the cluster upon the addition of one oxygen atom. Furthermore, the IEs of the dissociative and associative structures of $RhHo_2O_2$ were found to differ by 0.26 eV.

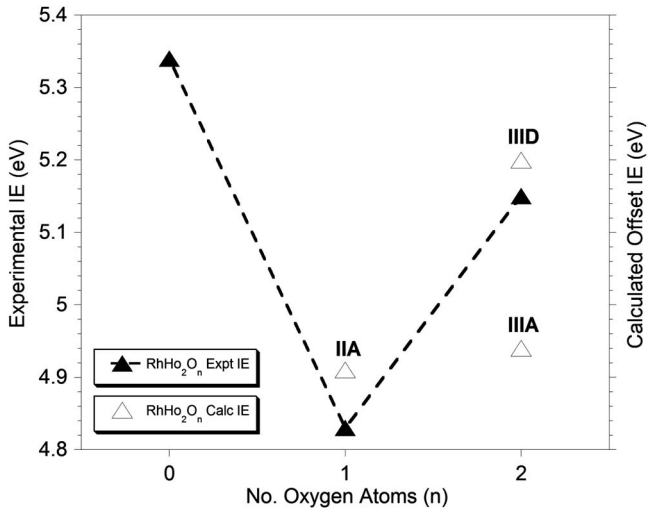

FIG. 5. Graph showing the experimental IE values for the $RhHo_2O_n$ (n=0–2) clusters as a function of constituent oxygen atoms. Also shown are the offset IE values calculated using DFT. Note that the "calculated offset" value for $RhHo_2$ is arbitrarily set to the experimental value and this difference is used as the offset correction for the other calculated IE values. The isomer of each cluster that represents each IE value has also been labeled.

D. Comparison between experimental and theoretical data

As with previous studies by our group, the theoretical IEs are determined to be higher in energy than the experimentally determined IEs.[42–44] This is attributed to the nature of the B3P86 functional. Therefore, the IEs are corrected with respect to the $RhHo_2$ bare metal cluster as we are primarily concerned with how the IE changes with respect to the sequential addition of oxygen atoms. The difference between the calculated and experimental IE of $RhHo_2$ was determined to be +0.46 eV. This difference is then applied to $RhHo_2O$ and $RhHo_2O_2$ to give the offset IE values that are listed in the final column of Table II.

Figure 5 shows the experimental and offset IEs plotted against the number of constituent oxygen atoms for each cluster. The general trend in IE as a function of oxygen atoms is observed to be the same in both sets of data; both show that the addition of one oxygen atom redshifts the IE. The difference between the experimental and offset IE is only +0.09 eV for $RhHo_2O$. Upon the addition of two oxygen atoms to $RhHo_2$, the offset IE for the dissociative structure compares better with the experimental IE (+0.07 eV difference) than the associative structure (−0.19 eV difference). This implies that the $RhHo_2O_2$ species that we detect in our experiment is a dissociative structure, which is supported by the relative energy calculations, which show that the associative structure is +4.01 eV higher in energy than the dissociative structure.

Finally, the good comparison between the experimental and theoretical data in Fig. 5 also indicates that our computational method of incorporating the f-electrons into the ECP is valid. This implies that f-electrons play no significant part in the electron density that is removed following the ionization of transition-lanthanide bimetallic clusters.

V. CONCLUSIONS

We determined the experimental IEs of the rhodium-holmium bimetallic clusters $RhHo_2O_n$ (n=0–2) using PIE spectroscopy. We find the IE of $RhHo_2O$ to be significantly red-shifted in comparison to the IEs of $RhHo_2$ and $RhHo_2O_2$, which are similar. We also determined the lowest energy structures for both the neutral and cationic $RhHo_2O_n$ (n=0–2) clusters using DFT and calculated the theoretical adiabatic IEs from these structures. We find the values to compare extremely well with the experimental values, allowing us to infer geometric information for each cluster. From this, we contend that the lowest energy neutral structures

calculated for each cluster are the most likely isomers present in the molecular beam upon ionization. In particular, we find the calculated adiabatic IE for the dissociative $RhHo_2O_2$ structure to compare better with the experimental value than the corresponding lowest energy associative structure. The good comparison between both sets of IE data also indicates that *f*-electrons seem to play no significant role in the valence electrons of transition-lanthanide bimetallic clusters.

ACKNOWLEDGMENTS

Financial support from the University of Adelaide's Faculty of Sciences is gratefully acknowledged. Support from the Australian Research Council for the purchase and maintenance of the lasers is also acknowledged. Computing resources provided by the National Computational Infrastructure (NCI) Facility and eResearch SA is also gratefully acknowledged.

[1] Metal Oxides, in *Chemistry and Applications*, edited by J. L. G. Fierro (CRC, Taylor & Francis, Boca Raton, 2006).
[2] K. J. Zhen, M. M. Khan, C. H. Mak, K. B. Lewis, and G. A. Somorjai, J. Catal. **94**, 501 (1985).
[3] M. M. Khan and G. A. Somorjai, J. Catal. **91**, 263 (1985).
[4] A. T. Ashcroft, A. K. Cheetham, J. S. Foord, M. L. H. Green, C. P. Grey, A. J. Murrell, and P. D. F. Vernon, Nature (London) **344**, 319 (1990).
[5] G. Fu, X. Xu, X. Lu, and H. L. Wan, J. Phys. Chem. B **109**, 6416 (2005).
[6] G. Fu, X. Xu, X. Lu, and H. L. Wan, J. Am. Chem. Soc. **127**, 3989 (2005).
[7] G. Fu, X. Xu, and H. L. Wan, Catal. Today **117**, 133 (2006).
[8] R. A. J. O'Hair and G. N. Khairallah, J. Cluster Sci. **15**, 331 (2004).
[9] Y. Shi and K. M. Ervin, J. Chem. Phys. **108**, 1757 (1998).
[10] J. Hagen, L. D. Socaciu, M. Elijazyfer, U. Heiz, T. M. Bernhardt, and L. Wöste, Phys. Chem. Chem. Phys. **4**, 1707 (2002).
[11] L. D. Socaciu, J. Hagen, T. M. Bernhardt, L. Wöste, U. Heiz, H. Hakkinen, and U. Landman, J. Am. Chem. Soc. **125**, 10437 (2003).
[12] T. Waters, R. A. J. O'Hair, and A. G. Wedd, J. Am. Chem. Soc. **125**, 3384 (2003).
[13] J. A. Rodriguez, Surf. Sci. Rep. **24**, 223 (1996).
[14] E. Janssens, G. Santambrogio, M. Brummer, L. Wöste, P. Lievens, J. Sauer, G. Meijer, and K. R. Asmis, Phys. Rev. Lett. **96**, 233401 (2006).
[15] Å. Slagtern and U. Olsbye, Appl. Catal., A **110**, 99 (1994).
[16] G. M. Koretsky and M. B. Knickelbein, Eur. Phys. J. D **2**, 273 (1998).
[17] Z. A. Reed and M. A. Duncan, J. Phys. Chem. A **112**, 5354 (2008).
[18] J. Suzumura, N. Hosoya, S. Nagao, M. Mitsui, and A. Nakajima, J. Chem. Phys. **121**, 2649 (2004).
[19] T. Kurikawa, Y. Negishi, F. Hayakawa, S. Nagao, K. Miyajima, A. Nakajima, and K. Kaya, Eur. Phys. J. D **9**, 283 (1999).
[20] S. Nagao, Y. Negishi, A. Kato, Y. Nakamura, A. Nakajima, and K. Kaya, J. Phys. Chem. A **103**, 8909 (1999).
[21] S. Nagao, Y. Negishi, A. Kato, Y. Nakamura, A. Nakajima, and K. Kaya, J. Chem. Phys. **117**, 3169 (2002).
[22] T. Durakiewicz and S. Halas, Chem. Phys. Lett. **341**, 195 (2001).
[23] Y. H. Luo and Y. Z. Wang, Phys. Rev. A **64**, 015201 (2001).
[24] Z. J. Wu, W. Guan, J. Meng, and Z. M. Su, J. Cluster Sci. **18**, 444 (2007).
[25] Z. J. Wu, J. S. Shi, S. Y. Zhang, and H. J. Zhang, Phys. Rev. A **69**, 064502 (2004).
[26] D. B. Zhang and J. Shen, J. Chem. Phys. **120**, 5104 (2004).
[27] D. B. Zhang, J. Shen, and N. X. Chen, J. Chem. Phys. **123**, 154213 (2005).
[28] N. Liu, Q. M. Ma, Z. Xie, Y. Liu, and Y. C. Li, Chem. Phys. Lett. **436**, 184 (2007).
[29] D. L. Cocke and K. A. Gingerich, J. Phys. Chem. **75**, 3264 (1971).
[30] D. L. Cocke and K. A. Gingerich, J. Phys. Chem. **76**, 2332 (1972).
[31] N. Veldeman, E. Janssens, K. Hansen, J. De Haeck, R. E. Silverans, and P. Lievens, Faraday Discuss. **138**, 147 (2008).
[32] Y. Q. Huang and B. S. Freiser, J. Am. Chem. Soc. **110**, 387 (1988).
[33] J. K. Gibson, J. Phys. Chem. **100**, 507 (1996).
[34] A. Fukuoka, L.-F. Rao, N. Kosugi, H. Kuroda, and M. Ichikawa, Appl. Catal. **50**, 295 (1989).
[35] R. Wesendrup and H. Schwarz, Organometallics **16**, 461 (1997).
[36] W. A. Weber and B. C. Gates, J. Catal. **180**, 207 (1998).
[37] A. M. Argo and B. C. Gates, J. Phys. Chem. B **107**, 5519 (2003).
[38] A. Ishikawa and E. Iglesia, J. Catal. **252**, 49 (2007).
[39] S. Gilb, M. Arenz, and U. Heiz, Low Temp. Phys. **32**, 1097 (2006).
[40] D. F. Shriver, P. W. Atkins, T. L. Overton, J. P. Rourke, M. T. Weller, and F. A. Armstrong, *Inorganic Chemistry* (Oxford University Press, Oxford, 2006).
[41] S. Nonose, Y. Sone, K. Onodera, S. Sudo, and K. Kaya, J. Phys. Chem. **94**, 2744 (1990).
[42] V. Dryza, J. R. Gascooke, M. A. Buntine, and G. F. Metha, Phys. Chem. Chem. Phys. **11**, 1060 (2009).
[43] V. Dryza, M. A. Addicoat, J. R. Gascooke, M. A. Buntine, and G. F. Metha, J. Phys. Chem. A **112**, 5582 (2008).
[44] V. Dryza, M. A. Addicoat, J. R. Gascooke, M. A. Buntine, and G. F. Metha, J. Phys. Chem. A **109**, 11180 (2005).
[45] M. J. Frisch, G. W. Trucks, H. B. Schlegel *et al.*, GAUSSIAN 03, Revision E.01, Gaussian, Inc., Wallingford, CT, 2004.
[46] M. Dolg and H. Stoll, Theor. Chim. Acta **75**, 369 (1989).
[47] M. Dolg, H. Stoll, and H. Preuss, Theor. Chim. Acta **85**, 441 (1993).
[48] M. Dolg, H. Stoll, and H. Preuss, THEOCHEM **277**, 239 (1992).
[49] M. Dolg, H. Stoll, A. Savin, and H. Preuss, Theor. Chim. Acta **75**, 173 (1989).
[50] See EPAPS Document No. E-JCPSA6-130-057916 for energetic and structural information of each respective cluster. For more information on EPAPS, see http://www.aip.org/pubservs/epaps.html.
[51] M. R. Zakin, D. M. Cox, and A. Kaldor, J. Chem. Phys. **89**, 1201 (1988).
[52] A. V. Nemukhin, A. Y. Ermilov, M. A. Petrukhina, W. E. Klotzbucher, and J. Smets, Spectrochim. Acta, Part A **53**, 1803 (1997).
[53] S. P. Willson and L. Andrews, J. Phys. Chem. A **103**, 6972 (1999).
[54] A. Gatterer, Ric. Spettroscop. **1**, 139 (1942).
[55] M. Dulick, E. Murad, and R. F. Barrow, J. Chem. Phys. **85**, 385 (1986).
[56] E. Murad and D. L. Hildenbrand, J. Chem. Phys. **73**, 4005 (1980).
[57] R. J. Ackermann, E. G. Rauh, and R. J. Thorn, J. Chem. Phys. **65**, 1027 (1976).
[58] A. Citra and L. Andrews, J. Phys. Chem. A **103**, 4845 (1999).
[59] J. B. Pedley and E. M. Marshall, J. Phys. Chem. Ref. Data **12**, 976 (1983).
[60] Y.-M. Chen and P. B. Armentrout, J. Chem. Phys. **103**, 618 (1995).
[61] G. J. Mains and J. M. White, J. Phys. Chem. **95**, 112 (1991).